North Atlantic Subtropical Mode Water properties: Intrinsic and atmospherically-forced interannual variability

Olivier Narinc[1], Thierry Penduff[1], Guillaume Maze[2], Stéphanie Leroux[3], and Jean-Marc Molines[1]

[1]Université Grenoble Alpes, CNRS, INRAE, IRD, Grenoble INP, Institut des Géosciences de l'Environnement (IGE), Grenoble, France.
[2]Univ Brest, Ifremer, CNRS, IRD, LOPS, F-29280 Plouzané, France
[3]Datlas, Grenoble, France.

Correspondence: Thierry Penduff (Thierry.Penduff@cnrs.fr)

Abstract. This study investigates the contributions of the ocean's chaotic intrinsic variability (CIV) and atmospherically-forced variability on the interannual fluctuations of the North Atlantic Subtropical Mode Water (STMW) properties. Utilizing a 1/4° regional 50-member ocean/sea-ice ensemble simulation driven by an original surface forcing method and perturbed initially, the forced variability of STMW properties is estimated from ensemble mean fluctuations, while CIV is determined from deviations around the ensemble mean within each member. The model successfully captures the main features of STMW, showing correct agreement with observation-based ARMOR3D data in terms of location, seasonality, mean temperature and volume, and interannual variance of its main properties. CIV significantly impacts STMW, explaining 10-13 and 28-44 % of the interannual variance of its geometric and thermohaline mean properties, respectively, with a maximum imprint on STMW temperature. Observation-based and simulated intrinsic-to-total variance ratios are mostly consistent, dispelling concerns about a signal-to-noise paradox. This study also illustrates the advantages of ensemble simulations over single simulations in understanding oceanic fluctuations and attributing them to external drivers, while also cautioning against overreliance on individual simulations assessments.

1   Introduction

The North Atlantic Subtropical Mode Water (STMW), also called Eighteen Degree Water (~~STMW~~EDW), is an abundant water mass located in the North Atlantic subtropical gyre. It is a weakly stratified, homogeneous water mass sitting on top of the permanent pycnocline with constant temperature near 18°C (Worthington, 1958; Feucher et al., 2016). The STMW plays a notable role in climate and ecosystems, most notably because it is a significant heat and anthropogenic carbon reservoir (e.g. Dong and Kelly, 2004; Bates et al., 2002; Bates, 2007; Kelly et al., 2010; Pérez et al., 2013) that further supply or deplete oxygen and nutrients to the subtropical gyre and the Western boundary current system (e.g. Jenkins and Doney, 2003; Palter et al., 2005). Worthington (1958) first described a possible formation mechanism for STMW, later completed in Worthington (1976): surface buoyancy loss during the winter deepens the mixed layer in the Gulf Stream area. Part of this newly formed water mass is advected eastward by the North Atlantic Current, but most of it is subducted in spring to the south and isolated from the atmosphere below the summer thermocline. This subduction process forms the weakly stratified core of STMW, which

is partially renewed each year. Maze et al. (2009); Forget et al. (2011); Billheimer and Talley (2013, 2016); Joyce et al. (2013) and Joyce (2013) among others have shown that the seasonal fluctuations of STMW are governed by air-sea fluxes that form the deep winter mixed layer feeding the STMW reservoir, and vertical diffusion together with isopycnal eddy-driven mixing to the south of the Gulf Stream that erode the STMW reservoir. More recently, Wenegrat et al. (2018) have shown that submesoscale eddies through near-surface restratification (mixed layer instability) can significantly erode the STMW reservoir. However, Sinha et al. (2023) have shown that mesoscale-resolving numerical simulations can capture this impact without fully-resolved submesoscales (i.e. buoyancy fluxes insensitive to finer grid resolution).

Mode waters are associated with minima in Ertel Potential Vorticity (PV), where relative vorticity ζ is generally omitted when the available data have coarse spatial resolution. Forget et al. (2011) and Joyce (2013) have noted that while PV minima are very often used to detect STMW, there is no unique definition of this water mass in the literature. Depending on their available data, authors use working definitions that identify STMW well enough for their purposes. Drawing on the impermeability theorem laid out by Haynes and McIntyre (1990), Marshall et al. (2001) showed that there can be no PV flux across isopycnals within the water column, and that any PV flux along isopycnals can only take place at the air-sea interface or at the interface with topography. Since STMW is formed in the winter mixed layer, it is visible as a pool of low PV relative to its surroundings once isolated from the atmosphere below the seasonal thermocline, and any erosion of this low PV pool must be isopycnal. Using 3-dimensional data obtained from observations or numerical simulations, it is possible to combine PV and density to identify and describe the STMW (*e.g.* Maze and Marshall (2011)).

Kwon and Riser (2004) have shown that the observed interannual-to-decadal fluctuations of STMW properties are strongly correlated to the North Atlantic Oscillation index. Dong and Kelly (2013) used a combination of observations and proxies for key processes (e.g. Gulf Stream path length for mixing) to further investigate these low-frequency fluctuations and highlighted the dominant role of surface heat fluxes, Ekman advection playing a smaller but non-negligible role. Evans et al. (2017) and Li et al. (2022) further demonstrated that STMW interannual volume variations are indeed driven by a combination of diabatic and adiabatic atmospheric forcing, but that the NAO-related adiabatic forcing (Ekman-driven) is a key player to explain local extreme anomalies.

However, model studies have shown that STMW interannual fluctuations are not fully explained by the atmospheric variability when oceanic non-linearities are explicitly simulated. Hazeleger and Drijfhout (2000) showed from shallow-water eddying simulations that the horizontal distribution of the STMW thickness exhibits modes of interannual variability under climatological atmospheric forcing devoid of interannual fluctuations. Dewar (2003) further showed from quasi-geostrophic eddying simulations that interannual to multidecadal modes of variability also emerge under stochastic atmospheric forcing in the region of the STMW. These low-frequency modes emerge in the absence of any low-frequency atmospheric variability and may thus be labelled *intrinsic*. More realistic, primitive equation ocean simulations confirmed the emergence and persistence in the eddying regime of substantial low-frequency intrinsic variability under seasonal forcing (Penduff et al., 2011), with marked imprints on the North Pacific STMW as well (Douglass et al., 2012). Various non-linear oceanic processes have been invoked to explain this phenomenon. Sérazin et al. (2018) for instance showed that an inverse cascade of kinetic energy from mesoscale turbulence towards larger scales can drive intrinsic variability up to interannual timescales, regardless of the atmospheric vari-

ability; Hochet et al. (2020) showed from eddying simulations that large-scale baroclinic instabilities may also directly generate
interannual-to-decadal intrinsic variability with no direct contribution of mesoscale turbulence. However, Penduff et al. (2011)
and Grégorio et al. (2015) showed that the interannual-to-multidecadal intrinsic variability becomes negligible when the reso-
lution of their global ocean model is coarsened from $\frac{1}{4}^{\circ}$ to $2°$.

The large ensemble of global ocean/sea-ice simulations performed during the OceaniC Chaos – ImPacts, strUcture, pre-
dicTability (OCCIPUT) project (Penduff et al., 2014) has shown that at $\frac{1}{4}^{\circ}$ resolution, intrinsic variability can compete with,
and locally exceed, its atmospherically-forced counterpart at interannual-to-decadal timescales, with substantial imprints on
many large scale oceanic indices: Atlantic Meridional Overturning Circulation (Leroux et al., 2018), global Meridional Heat
Transport (Zanna et al., 2019), latitude and velocity of the Kurushio extension (Fedele et al., 2021), Southern Ocean eddy
kinetic energy (Hogg et al., 2022), Ocean Heat Content variability and long-term trends (Sérazin et al., 2017; Llovel et al.,
2022), etc. These studies highlight the random phase of intrinsic ocean fluctuations developing within individual ensemble
members around the atmospherically-paced ensemble mean evolution. This nonlinearly-driven random ocean variability will
thus be referred to here as Chaotic Intrinsic Variability (CIV).

Since Hazeleger and Drijfhout (2000) and Dewar (2003), no study has been published on the North Atlantic STMW chaotic
intrinsic variability. During the last 20 years however, model studies have confirmed in idealized and realistic setups that mid-
latitude ocean dynamics are strongly impacted by low-frequency CIV in particular within western boundary current systems
and their associated recirculation gyres, where STMW is found. The major contribution of non-linear and mesoscale processes
in STMW formation and erosion is also well established. It is thus time to revisit and quantify the relative contributions of
CIV and of atmospheric fluctuations in the interannual STMW variability; this is the aim of the present study, performed with
a primitive equation ensemble simulation, whose realism will be assessed against an observational reference.

Section 2 describes the simulated and observation-based datasets used in this study, our definitions of STMW and of its
features, and the methods we used to process the data. Section 3 compares the simulated and observation-based STMW in-
terannual variabilities, and assesses their forced and chaotic intrinsic components with a highlight on ensemble simulation
benefits. Our results are summarized and discussed in Section 4.

2   Datasets and processing

2.1   The OCCIPUT regional ocean/sea-ice ensemble simulation

2.1.1   Ensemble modelling strategy

Our 5-daily model dataset was produced during the OCCIPUT project using a 50-member regional ensemble of forced oceanic
hindcasts performed with the NEMO v3.5 ocean/sea-ice model implemented on the North Atlantic with 1/4° horizontal reso-

lution and 46 vertical levels[1]-. This regional ensemble simulation, referred to as NATL025-GSL301 in the OCCIPUT database, is similar to the E-NATL025 simulation described in Bessières et al. (2017) with two differences: its size (50 members instead of 10) and its atmospheric forcing function, as described below. Its southern and northern boundaries at 20°S and 80°N are treated as solid walls with 28-gridpoint buffer zones where simulated tracers are restored to monthly climatological conditions (Levitus et al., 1998), with a restoring coefficient decreasing inwards toward zero; intrinsic variability is therefore solely generated inside the domain without any influence coming from the surrounding ocean, and damped in the buffer zones.

The 50 ensemble members are initialized on January 1st, 1993 from the final state of a single-member 19-year spin-up, and are further integrated for 20 years until the end of 2012. The ensemble dispersion is triggered by applying a slight stochastic perturbation within each member during 1993; this perturbation scheme is described in Brankart (2013) and is designed to simulate the impact of subgrid-scale uncertainty on geostrophic velocities. The perturbations are turned off at the end of 1993, and the spread that they have introduced is then fully controlled by nonlinear ocean processes during the rest of the run. The realistic Drakkar Forcing Set DFS5.2 described in Dussin et al. (2016) is used between 1993 and 2012 to derive the atmospheric forcing, which is applied identically on all ensemble members: the (atmospherically-)*forced* variability is thus estimated from the variability of the ensemble mean, and the *CIV* is given by deviations around the ensemble mean within each ensemble member. The technical implementation of OCCIPUT ensembles is described in more detail in Bessières et al. (2017).

2.1.2 The ensemble-averaged forcing function and its impact on ensemble statistics

Besides its regional extension and shorter duration, this simulation differs from the 56-year global OCCIPUT ensemble described in earlier papers (e.g. Bessières et al., 2017) by its surface forcing: all members are forced by identical air-sea fluxes in our regional ensemble, rather than identical atmospheric conditions in the global ensemble. At each timestep, bulk formulae are used within each of the 50 regional members to compute air-sea fluxes based on the current DFS5.2 atmospheric state and on each member's surface state. The ensemble average of these air-sea fluxes is then computed at each time step, and applied uniformly on all members in order to compute the next time step.

Figure 1 compares in the STMW pool the behaviour of the present ensemble (with ensemble-averaged air-sea fluxes)with a smaller 10-member ensemble, where each member was driven by air-sea fluxes computed from its own surface state[1]; the latter 10-member ensemble run was referred to as E-NATL025 and described in Bessières et al. (2017). The left panel in Figure 1 shows that the shallowest maximum of model stratification (in ensemble and temporal average) sits at the depth (about 50 m) of the seasonal pycnocline, and above the pool of weakly stratified STMW found between about 150 and 300 m. The second stratification maximum locates the permanent pycnocline at about 450 m on average, and the stratification decreases towards greater depths. This profile is not only consistent with the observed mean stratification of the region (e.g. Feucher

---

[1]This regional ensemble simulation, referred to as NATL025-GSL301 in the OCCIPUT database, is similar to the E-NATL025 simulation described in Bessières et al. (2017) with two differences: its size (50 members instead of 10) and its atmospheric forcing function, as described below. The technical implementation of OCCIPUT ensembles is described in detail in the latter paper.

[1]This 10-member ensemble run is referred to as E-NATL025 and described in Bessières et al. (2017).
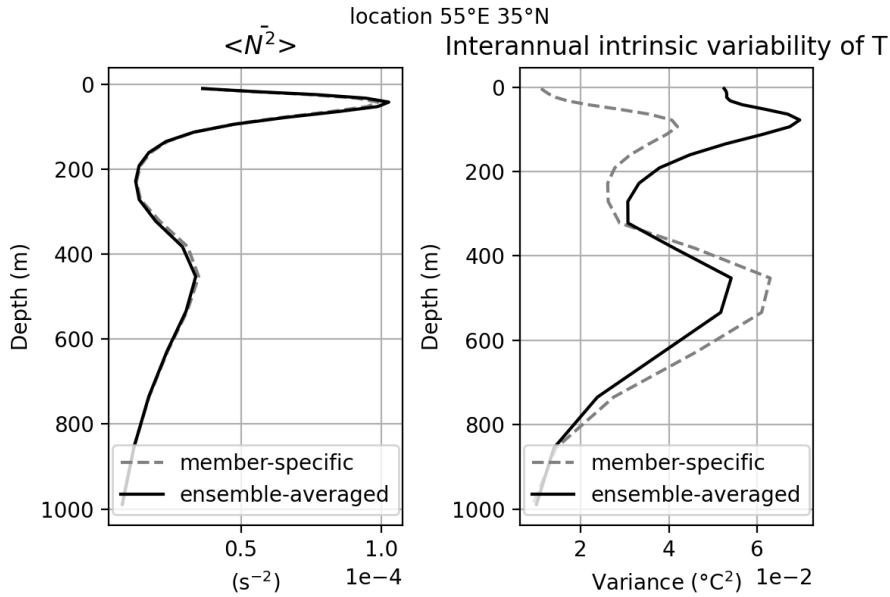
Figure 1. Vertical profiles of the time- and ensemble-averaged Brunt-Väisälä frequency (left), and of the time-average of the ensemble variance of yearly mean temperature (right). Results are shown for the run where ensemble-averaged air-sea fluxes are applied to all members (thick line), and for the run where member-specific air-sea fluxes are applied to each member (dashed line). All profiles are taken at the same location within the formation zone of STMW.

et al., 2016, 2019), but is almost identical in both ensembles: these two results show the equal consistency and realism of both forcing methods regarding the main STMW structure, and of the ensemble mean (forced) long-term model state.

The vertical profile of interannual intrinsic variance of temperature ($varT(z)$, right panel in Figure 1) has the same general shape as the averaged stratification in both ensembles, with the shallowest $varT$ maximum sitting slightly below the seasonal pycnocline. However, $varT$ at the surface increases by a factor of 5 when member-specific air-sea fluxes are replaced by ensemble-averaged fluxes; this factor is about 1.75 near the seasonal pycnocline[1]. In other words, using ensemble-averaged instead of member-specific air-sea fluxes does not adversely affect the atmospherically-forced oceanic state and evolution, and enhances the ensemble dispersion of yearly temperatures in the upper 300 m. We explain this latter enhancement and argue that this ensemble-averaged forcing method is preferable, as follows.

The classical (member-specific) computation of turbulent air-sea fluxes through bulk formulae in ocean-only simulations induces an implicit relaxation of sea-surface temperature (SST) toward a prescribed and fluctuating equivalent air temperature T_a, with a time scale on the order of 40 days in our region of interest (see Fig. 6 in Barnier et al. (1995)). (see Fig. 6 in Barnier et al., 1995)

---

[1]$varT$ below about 800 m and the full-depth stratification remain insensitive to the forcing method, but member-specific fluxes increase $varT$ by about 20% near the permanent pycnocline. This increase may be associated with the excessive damping of intrinsic baroclinic modes that account for SST fluctuations at the surface, and a subsequent enhancement of the baroclinic modes that explain temperature variability near the pycnocline. This hypothesis is currently under examination.

. This relaxation is arguably overestimated in such simulations where the heat capacity of the atmosphere is assumed infinite despite its being much smaller than that of the ocean in nature. In an ensemble simulation driven with member-specific fluxes, this results in SSTs being over-relaxed toward the same T_a within all members; this in turns yields an excessive damping of ensemble SST dispersion at these long timescales in particular, and of intrinsic variability in general. Indeed, previous 1/4°-resolution NEMO simulations driven by classical (member-specific) forcing have been shown to underestimate surface intrinsic variability at all scales , compared to observations ~~and to 1/12° simulations (see e.g. Penduff et al., 2010; Sérazin et al., 2015, 2018).~~ (see e.g. Penduff et al., 2010). The use of ensemble averaged fluxes enhances surface intrinsic variability and compensates for this bias.

The ensemble-averaged forcing method avoids this excessive damping of surface CIV and lets intrinsic temperature anomalies reach up to the surface. Such a behavior is arguably expected in coupled ocean-atmosphere simulations, where the ocean's thermal inertia overwhelms that of the atmosphere; estimating the strength of interannual CIV in eddying coupled models would help verify this hypothesis. Nevertheless, the use of ensemble-averaged instead of member-specific fluxes removes this unphysical imbalance between the oceanic and atmospheric heat capacities, and compensates the lack of simulated intrinsic variability. ~~We~~

Intrinsic thermal anomalies are not damped with the ensemble averaged forcing approach; such anomalies in the real ocean may be slightly damped by air-sea interactions, but much less strongly than in the member-specific approach. We thus hypothesize that the amplitude of upper-ocean temperature interannual CIV in nature sits between those simulated with both forcing strategies, and argue that the ensemble-averaged forcing method lets it evolve in a more physically-consistent and realistic way.

2.2 The ARMOR3D gridded observational product

We use ARMOR3D over its first 34 vertical levels (i.e. down to about 800 m) to assess the model simulation over our region of interest and the whole simulation period. ARMOR3D is a global analysis based on observational datasets including satellite sea surface temperature (SST), altimeter-derived sea surface height, in-situ temperature/salinity profiles from the Argo array, CTD and XBT profiles. These observations were processed to provide temperature (T), salinity (S), and geostrophic velocity (u,v) fields on a 3-D grid at 1/4° resolution using optimal interpolation and multiple linear regression methods as explained in Guinehut et al. (2012) and Mulet et al. (2012). This latter study presents how gridded T and S fields are used to provide consistent 3-D velocity fields via the thermal wind relation, with a surface reference level where geostrophic velocities are derived from altimetry.

ARMOR3D has some uncertainties and limitations, as any gridded product constrained by observations. Episodic spurious density inversions have been detected in ARMOR3D near the surface (E. Pauthenet, personal communication), but these artifacts do not affect the subsurface where most of the STMW is found. The interannual variability (in particular of salinity) is also known to be somewhat underestimated in ARMOR3D (Guinehut et al., 2012), partly since the coverage of in-situ data is relatively coarse and since optimal interpolation has a tendency to smooth solutions.

The ARMOR3D dataset also has strengths despite its limitations, and it was chosen as our observation-based reference for three main reasons, the first two of which are documented in Balmaseda et al. (2015): [i] ARMOR3D compares well with

independent observations at local and large-scale in our region of interest, with a skill that is similar to ocean reanalyses. [ii] The ARMOR3D fields are independent of multiple and complex modelling choices, which produce substantial differences between reanalyses. [iii] Perhaps more decisively, ARMOR3D is the only available model-independent T,S,u,v dataset that yields the full Ertel PV (including ζ) at a spatiotemporal resolution that is close to that of our model. As in all comparisons between simulations and any observation-based gridded dataset, the specificities of ARMOR3D will be taken into account in the comparisons discussed below.

2.3 ARMOR3D and simulated mean seasonal STMW structure

Ertel PV (Ertel, 1942) is defined as $Q = \frac{1}{\rho_0}(\zeta + f) \cdot \frac{\partial \rho}{\partial z}$, where f is the Coriolis parameter, ρ is potential density, ρ_0 is a reference density, and ζ is relative vorticity; given the relatively fine resolution (1/4°) of our multivariate datasets, we do not neglect this latter term. In the rest of this paper, figures and numerical values express PV as $\rho_0 Q$ (in $\mathrm{kg\,m^{-4}\,s^{-1}}$), which is Ertel PV normalised by $\rho_0 = 1020\ \mathrm{kg\,m^{-3}}$. Figures 2 and 3 show meridional sections of seasonally-averaged PV in one randomly chosen ensemble member and in ARMOR3D. We verified that the behavior of this particular member is representative of all members in the ensemble, and that the following is robust.

Two mean biases appear in these sections: the simulated STMW is about 80 m shallower and 0.4 $\mathrm{kg\,m^{-3}}$ lighter than in ARMOR3D, and its density range is wider (i.e. its PV is larger). This may be explained by a 0.4 psu fresh bias in the simulated STMW in temporal and ensemble average, and by the usual tendency of this class of models to overestimate vertical mixing.

However, multi-year animations of these fields in various ensemble members and in ARMOR3D confirm that in both datasets the wintertime deepening of the mixed layer feeds the STMW reservoir, which is then shielded from the atmosphere in summer. The main features of the simulated STMW seasonal cycle (location, properties, time of formation and subduction, etc) in the simulation are thus consistent with ARMOR3D and with those described in e.g. Maze et al. (2009); Kelly and Dong (2013); Billheimer and Talley (2016) and many other studies.

2.4 STMW definitions and properties

STMW identification criteria	Reference
Temperature in the 17-19 °C range	Worthington (1958)
Density within a certain range	Speer and Tziperman (1992)
Salinity in a certain range	Joyce (2013)
Potential vorticity below a maximum threshold	Forget et al. (2011), Maze and Marshall (2011)
Vertical gradient of temperature below a maximum threshold	Kwon and Riser (2004)
Geographic boundaries	Worthington (1976)

Table 1. Criteria used in the literature to define STMW and associated references. This list is non-exhaustive since similar criteria are used in other studies.
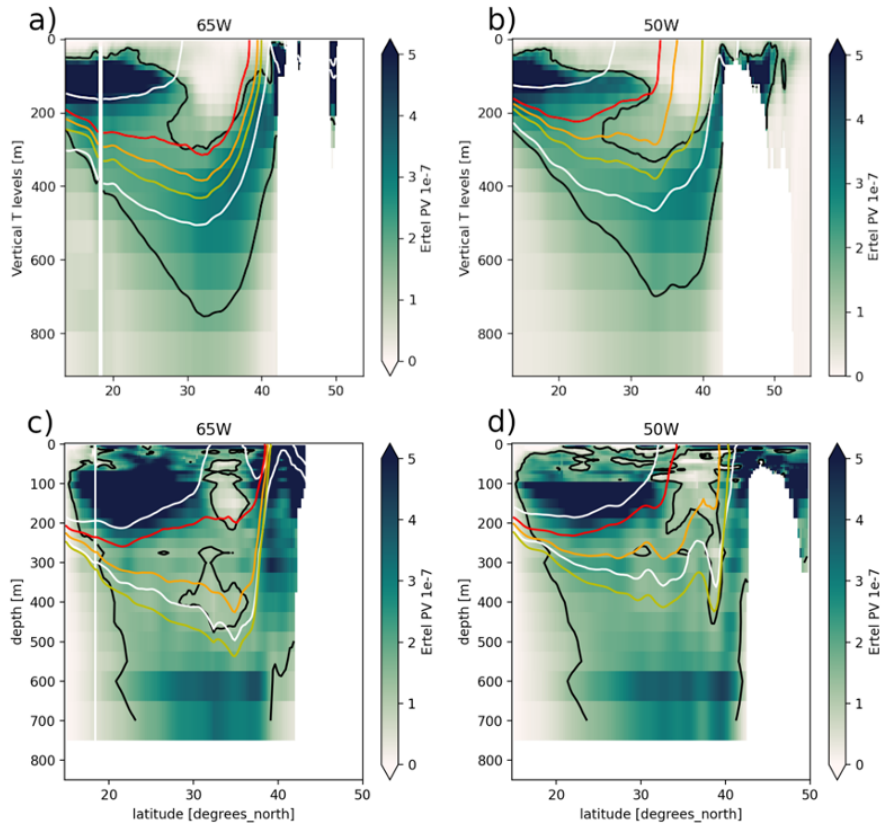
Figure 2. Sections at 65°W (left) and 50°W (right) of the winter Ertel PV, averaged over February-March-April from 1993 to 2012, in one ensemble member (top) and in ARMOR3D (bottom). Yellow, orange, and red lines show the 17, 18, and 19°C isotherms, respectively. White lines show the STMW density bounds in the model ($25.2 \leq \gamma \leq 26.4 \ \mathrm{kg\,m^{-3}}$) and in ARMOR3D ($25.8 \leq \gamma \leq 26.4 \ \mathrm{kg\,m^{-3}}$). Black lines show the STMW PV upper bound in the model ($\mathrm{PV} < 1.7 \cdot 10^{-7} \mathrm{kg\,m^{-4}\,s^{-1}}$) and in ARMOR3D ($\mathrm{PV} < 1.2 \cdot 10^{-7} \mathrm{kg\,m^{-4}\,s^{-1}}$).

185   As mentioned in the introduction, various authors define STMW in different ways given the data available to them, typically using one or a combination of the criteria listed in Table 1. In the present study, simulated and ARMOR3D STMW are defined using three criteria: PV maximum, geographic boundaries, and density range (see Table 2). This definition is commonly used, see *e.g.* Forget et al. (2011). The PV maximum and geographical boundaries select weakly stratified waters in the region of interest, and the density range excludes those located outside the layer located between the seasonal and main thermoclines.

190   The PV maximum and density range ~~and~~ have different values in the model ensemble and the observational product to account for their differences (see Section 2.3). The ARMOR3D gridding algorithm also yields some uncertainty as to which exact criteria should be chosen to identify STMW. This uncertainty was evaluated using various sets of values for PV and density:
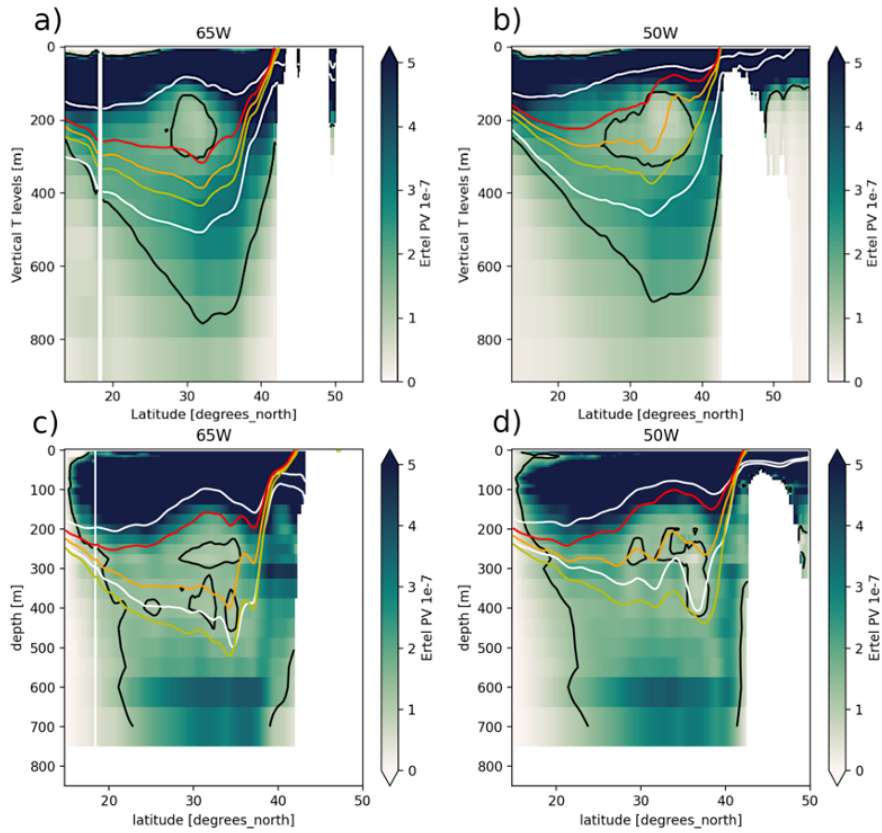
Figure 3. same as Figure 2 but for summer months (July-August-September).

	ARMOR3D	Ensemble simulation
Geographic boundaries	13 - 55°N, 36 - 82°W	13 - 55°N, 36 - 82°W
Neutral density range (γ in $kg \cdot m^{-3}$)	A: 25.8 - 26.4 / B: 25.74 - 26.46 / C: 25.68 - 26.54	25.2 - 26.4
Maximum PV ($10^{-7}kg \cdot m^{-4} \cdot s^{-1}$)	A:1.2 / B: 1.32 / C: 1.44	1.7

Table 2. Definition of STMW in the present study. A, B, and C correspond to sensitivity choices in ARMOR3D.

three of these are presented here, defined in Table 2 as A, B and C, with increasingly larger bounds. Section 3 evaluates the effect of the different values used in setting the boundaries of STMW in both datasets.

2.5 Computation and processing of STMW property time series

The above criteria are used within both datasets to label grid cells corresponding to STMW; their individual volumes are summed up at each time step to estimate the time-varying enclosed volume of STMW in Sv yr (i.e. volume arising from a 1 Sv flux sustained for 1 year: $31.536 \cdot 10^{12} \text{m}^3$). Model and ARMOR3D fields at labelled grid cells are then averaged to estimate the volume-weighted mean temperature (T), salinity (S), neutral density (γ), and PV of the simulated and ARMOR3D STMW. The mean depth of the water mass is finally given by the volume-weighted average of the immersions of labelled grid points.

The resulting time evolution of these 6 STMW properties may exhibit geophysical trends and variability at periods greater than the 20 years of available data, and potential numerical trends in the case of the simulation. Variability at periods longer than 20 years and possible trends were finally removed from each ensemble member and from ARMOR3D over the 20-year period using the LOWESS non-linear detrending method (Cleveland, 1979), yielding the evolution of STMW properties over the range of timescales T that is properly resolved in the datasets (10 d < T < 10 yr).

These 50+1 time series of each STMW property were further split over 2 ranges of time scales; [i] interannual time series (18 m < T < 10 yr) were obtained by removing the mean seasonal cycle from the 51 time series and applying a low-pass Lanczos filter with a cut-off period of 18 months; [ii] so-called subannual time series (10 d < T < 18 m, including seasonal cycles) were obtained by subtracting the interannual time series from the detrended time series.

2.6 Total, forced, and chaotic intrinsic variances

We hereafter focus on the contributions of the atmospherically-forced and chaotic intrinsic components of the STMW total interannual variability. The forced, intrinsic, and total variances (σ_F^2, σ_I^2 and σ_T^2, respectively) of any variable X are computed as in Leroux et al. (2018):

$$\sigma_F^2 = var_t(\langle X_m(t) \rangle) \tag{1}$$

$$\sigma_I^2 = \overline{var_m(X_m(t))} \tag{2}$$

$$\sigma_T^2 = \langle var_t(X_m(t)) \rangle \tag{3}$$

In the latter expressions, $\bar{\cdot} = \frac{1}{T}\sum_{t=1}^{T}$ is the temporal average over T time steps, $\langle \cdot \rangle = \frac{1}{M}\sum_{m=1}^{M}$ is the ensemble average of M members, $var_m(X_m(t)) = \frac{1}{M}\sum_{m=1}^{M}(X_m(t) - \langle X_m(t) \rangle)^2$ is the ensemble variance at time t, and $var_t(X_m(t)) = \frac{1}{T}\sum_{t=1}^{T}\left(X_m(t) - \overline{X_m(t)}\right)^2$ is the temporal variance for member m. It can be shown that with this choice of biased variance estimates, $\sigma_T^2 = \sigma_F^2 + \sigma_I^2$ if $\overline{X_m(t)} = 0$; this property is very well verified in our case since $|\frac{\sigma_T^2 - (\sigma_F^2 + \sigma_I^2)}{\sigma_T^2}| < 10^{-3}$. Finally, we estimate the intrinsic fraction of the total variance of STMW properties from the ratio $R_\sigma = 100\% \cdot \sigma_I^2/\sigma_T^2$.

3 Results

The interannual anomalies of integrated STMW properties defined in Section 2.5 are shown in Figure 4 for both datasets. The ensemble-and-temporal mean values of the STMW properties are given at the bottom of each panel for the simulation, and
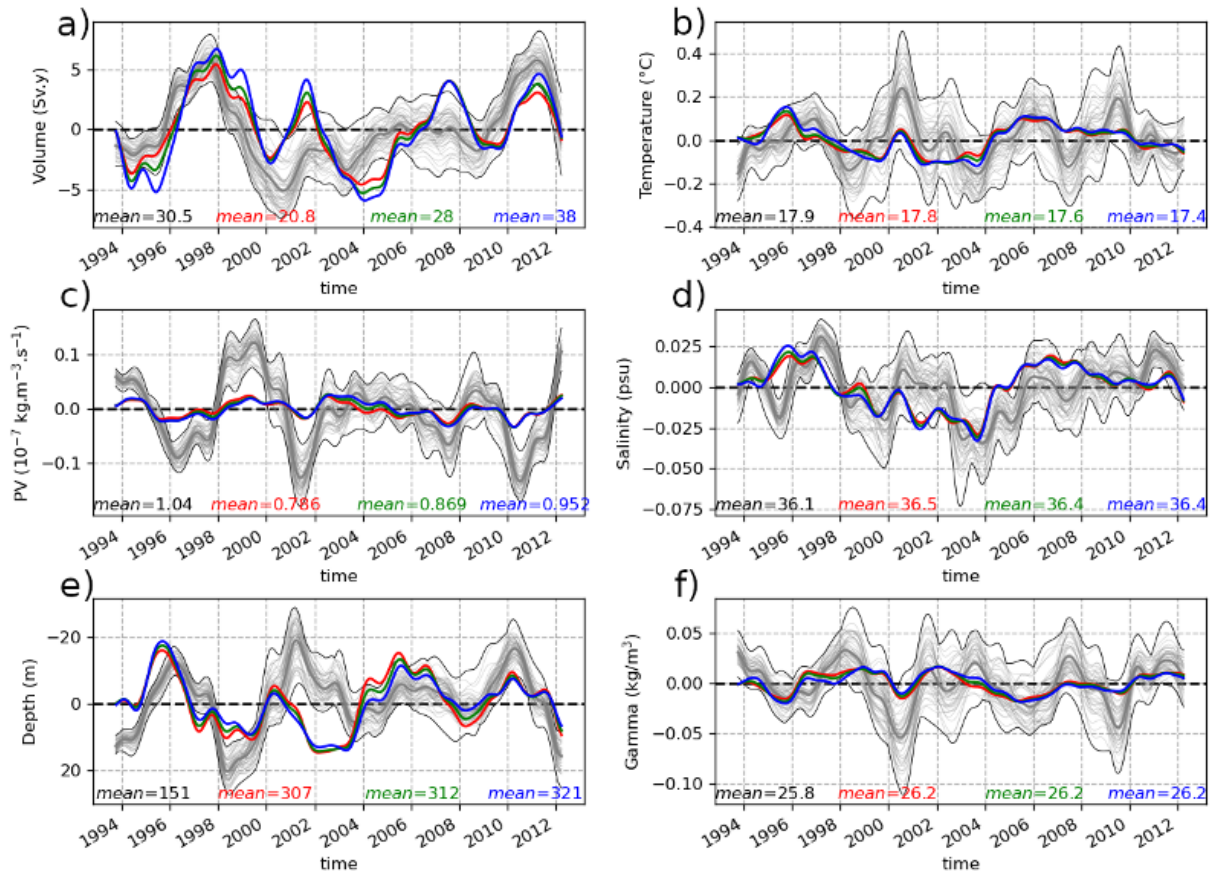
Figure 4. Interannual evolution of the six STMW property anomalies. Thin grey lines shows individual ensemble members, thick grey lines ensemble averages. Thin black lines show the maximum and minimum values of the entire ensemble at each time step. The coloured lines show the same quantities in ARMOR3D using the 3 definitions given in Section 2.2: criteria A, B, and C correspond to red, green, and blue lines, respectively. The text at the bottom gives the 1993-2012 mean value of STMW properties computed before detrending and filtering in the ensemble mean (black), and in the ARMOR3D data (same three colors as above).

225   for each of the three definitions in the observational product. Definition B in the observational product (green) yields a mean volume of 28 Sv.y that is very close to the 30.5 Sv.y in the ensemble, and will thus be retained in the following to identify STMW in ARMOR3D. The colored lines in this figure also show that in ARMOR3D, the 3 definitions of the STMW yield very similar interannual evolutions: this confirms the robustness of our criteria despite their partial arbitrariness.

      Simulated STMW properties vary around their ensemble mean within individual ensemble members, due to the random

230   phase of intrinsic variability in the 50 realizations. Throughout most of the integration period, the ARMOR3D-derived STMW interannual variability remains within the simulated envelope, providing a first indication of correct model-ARMOR3D agreement in terms of variability, which is assessed more precisely in the following.

	Temperature	Salinity	Density	Volume	PV	Depth
10 d < T < 10 yr	13.0	3.52	10.8	1.70	1.38	0.829
10 d < T < 18 m	4.94	1.71	3.53	0.333	0.471	0.261
18 m < T < 10 yr	44.1	24.8	38.4	13.2	10.6	13.0

Table 3. Intrinsic fraction of interannual variances (percentage $R_\sigma = 100\% \cdot \sigma_I^2/\sigma_T^2$) of STMW properties in three ranges of time scales T.

3.1 Forced and chaotic intrinsic components of the STMW variability

3.1.1 Intrinsic fraction of STMW properties' simulated variance

235 Using the definitions outlined in Section 2.4, we computed the intrinsic fraction R_σ of the variances of each simulated STMW property within the 3 ranges of timescales introduced in Section 2.5: all resolved periods (10 days to 10 years) and annual+subannual periods (10 days to 18 months), both of which include seasonal cycles, and interannual periods (18 months to 10 years). Results are shown in Table 3.

When all resolved timescales are considered (10 d < T < 10 yr), the contribution of intrinsic processes to the variance
240 of STMW properties reaches a modest maximum of 13% for temperature. This intrinsic fraction is even smaller at annual+subannual timescales with a maximum of 4.94% for temperature; the atmospheric forcing thus explains most of the variability of STMW properties at these relatively short timescales, consistently with the large control exerted by the atmospheric annual cycle on STMW (see Section 1).

Nonetheless, the intrinsic fraction gets much larger at interannual timescales. Even the smallest contributions of CIV (10.6
245 % for PV and about 13 % for volume and depth) cannot be neglected for 18 m < T < 10 yr. Interannual fluctuations of STMW thermohaline properties are most strongly impacted by CIV: about one fourth, one third, and one half of the interannual variance of STMW salinity, density, and temperature, respectively, is controlled by intrinsic processes and is random in phase. Explaining why interannual CIV has a weaker impact on "geometric" STMW properties (volume, PV and depth) would require additional analyses, which are left for future studies.

3.1.2 Simulated and ARMOR3D STMW fluctuations
250

STMW interannual fluctuations simulated in each member are compared to their ARMOR3D counterparts using Taylor diagrams (Taylor, 2001) in Figure 5. The reference for each simulated STMW property is the corresponding ARMOR3D interannual anomaly (based on definition B, see section 2.4): comparisons between each ensemble member and this reference yield 50 black dots in each panel.
255 The center of gravity (COG, blue square) of the black dots in the top left subpanel of Figure 5 sits very close to the unit radius circle: the ensemble-averaged total interannual STD of STMW volume compares very well with its ARMOR3D counterpart. In other words, the model remarkably simulates the interannual STD of the STMW volume in ARMOR3D in an ensemble averaged sense.

For the 5 other simulated STMW properties, ensemble-averaged interannual STDs exceed their ARMOR3D counterparts
by a factor of 1.2 for depth to 4.2 for PV. That our 1/4° ensemble may overestimate STMW fluctuations would come as a
surprise, since most NEMO simulations at this resolution rather tend to underestimate interannual fluctuations (see e.g. Penduff
et al., 2010). In fact, interannual fluctuations of simulated STMW properties are more in line than ARMOR3D estimates with
previous observational studies (see e.g. Fig. 2 and Fig. 2+S1 in Kwon and Riser, 2004; Stevens et al., 2020, respectively). It
is therefore very likely that we found here an illustration of ARMOR3D underestimating STMW fluctuations (especially for
PV), which is consistent with the fact that ARMOR3D is known to substantially underestimate the actual interannual ocean
variability (Guinehut et al., 2012).

We now focus on the ensemble dispersion of black dots around their COG in these panels. By design, all ensemble mem-
bers are driven by the same atmospheric evolution and simulate equally likely evolutions of STMW properties: inter-member
differences in STMW evolutions and in their agreement with ARMOR3D are thus due to different CIV realisations. Accord-
ingly, Figure 5 reveals a substantial angular dispersion of black dots with respect to the x axis, corresponding to differences in
correlations of individual ensemble members with ARMOR3D time series. For STMW volume for instance, certain ensemble
members have good phase agreement with the observational reference (up to 0.75 correlation) and almost the same interannual
STD, while other members have poorer correlations (as low as 0.4) and under- or over-estimate by 20% the ARMOR3D STD.
The CIV-related diversity of correlations and STD ratios is even larger for STMW temperature, whose interannual variance is
the most affected by CIV (Section 3.1): member-ARMOR3D correlations range from -0.45 to 0.79 and their STD ratios from
1.2 to 2.6.

These large dispersions indicate that slightly different initial conditions can strongly affect the skill of eddying ocean simu-
lations driven by the same realistic forcing for decades, yielding a wide range of model-ARMOR3D correlations of either sign
depending on the member considered. This demonstrates a specific value of ensemble experiments for model evaluation: this
approach gives a direct measure of the CIV-related uncertainty in simulated time series, and allows for a much more robust
model skill assessment.

For the six STMW properties under consideration, the green circles indicate how the ensemble mean (forced) variability
compares with the ARMOR3D reference. These circles show that the forced variability has smaller STD but is better correlated
with the reference than individual members in ensemble average (ensemble COG, blue squares). This is consistent with the
fact that the phase of CIV-related "noise" is random within each ensemble member: this noise is strongly attenuated in the
ensemble mean evolution, hence explaining the position of green dots relative to blue squares. On the other hand, the phase
of CIV in certain members may happen to correlate favorably (resp. defavorably) with the observational reference, explaining
that certain black dots sit right (resp. left) of the green lines; the same behavior was reported by Leroux et al. (2018) from the
analysis of AMOC fluctuations in the global OCCIPUT ensemble.

These results globally show relatively good agreement between the simulated and ARMOR3D data. The average and STD
of STMW volume is very similar in both datasets, other variables have an STD within the same order of magnitude (giving
the probable underestimation of ARMOR3D-derived estimates), and most ensemble means of STMW properties are in correct
phase agreement with ARMOR3D.

13

3.1.3 Possibility of a "signal-to-noise paradox"

We finally assess whether the simulated variability of STMW properties are affected by the so-called "Signal-to-Noise paradox", as discussed in Leroux et al. (2018). This concept has been proposed to characterize ensemble climate simulations where ensemble mean fluctuations are strongly correlated to observations, while most individual members are more closely correlated to other members than to observations (see e.g. Eade et al., 2014; Scaife and Smith, 2018; Christiansen, 2019). When this paradox is met, the ensemble mean (forced) variability is correctly simulated but the model is over-dispersive (overestimated contribution of CIV).

Figure 6 exhibits ~~for most STMW properties' interannual fluctuations significant overlaps between the blue and grey distributions, which correspond to~~ an overlap between the distributions of member-ARMOR3D correlations (blue) and member-member correlations ~~respectively~~(grey) for most interannual STMW properties. Member-ARMOR3D and member-member correlations overlap over the range 0.5–0.75 for STMW volume for instance, and over much wider ranges for STMW thermohaline properties. ~~Member-member~~ In particular, member-member correlations do not largely fall below member-ARMOR3D correlations, suggesting that the ensemble is not clearly over-dispersive~~; the~~. The opposite is however found for STMW depth, for which the ensemble seems to be under-dispersive. Besides this main exception though, we conclude that ~~no~~ it is unlikely that a signal-to-noise paradox contaminates the statistics of STMW properties in our simulation~~: in~~. In other words, the simulated partition between forced and intrinsic interannual variabilities of STMW properties are consistent with their counterparts in ARMOR3D.

4 Discussion and conclusion

We have investigated the contributions of the ocean's chaotic intrinsic variability (CIV) and of the atmospherically-forced variability in the interannual fluctuations of the North Atlantic Subtropical Model Water (STMW) main properties. We made use of a 1/4° regional 50-member ocean/sea-ice ensemble simulation with perturbed initial conditions, and of the ARMOR3D observation-based product. The forced variability of simulated STMW properties was estimated from the fluctuations of the ensemble mean, and its chaotic intrinsic variability from the deviations around the ensemble mean within each ensemble member. This regional ensemble simulation is driven through bulk formulae by a realistic atmospheric evolution, each member being forced by the same time-varying air-sea fluxes computed online via an ensemble average. We showed that this forcing approach avoids an excessive damping of the interannual CIV (i.e. ensemble spread) of upper ocean temperature, without impacting the mean state and forced variability.

Following the literature (Table 1), we identified the STMW in all ensemble members and in ARMOR3D using the same combination of physical criteria, i.e. all water parcels with low potential vorticity values within a geographical area and a density range. Parameters were adjusted to fit differences between the ARMOR3D and simulated mean states (Table 2). Geometric (volume, Ertel potential vorticity, depth) and thermohaline (temperature, salinity, density) properties of the STMW core were estimated from the simulation and from ARMOR3D over the period 1993-2012. We found that although slightly more buoyant,

the main features of the simulated STMW are in correct agreement with ARMOR3D, in particular its location, seasonality, mean temperature, mean volume and interannual volume variance (Figures 2 and 3).

The CIV contribution to the STMW properties' variance was estimated in different frequency bands via the intrinsic fraction R_σ. We found that STMW is substantially impacted by interannual CIV, which explains in particular 44 % of its low-frequency temperature variance. Explaining why thermohaline STMW properties are more impacted by interannual CIV than geometric STMW properties (R_σ = 28-44% vs. 10-13%, Table 3) would require a detailed analysis of the atmospheric and oceanic processes that control the water mass interannual evolution, which lies beyond the scope of the present paper and is left for the future. These results nevertheless provide a new context for the attribution of observed STMW fluctuations to external (atmospheric) and internal (oceanic) drivers: a non-negligible part (10-44 %) of STMW fluctuations is ocean-driven, random in phase, and cannot be explained by atmospheric fluctuations only.

We verified at interannual timescales that our analysis is not plagued by the so-called signal-to-noise paradox, such that intrinsic-to-total variance ratios are compatible in the ensemble simulation and in ARMOR3D (except for STMW depth, whose sensitivity to CIV may be underestimated in the model). These findings suggest that the contribution of CIV in the variance of real STMW properties is genuine, and globally consistent with its simulated contribution.

Building upon a few earlier studies (e.g. Leroux et al., 2018; Fedele et al., 2021), our present analysis illustrates the benefit of ensemble simulations over single hindcasts for model evaluation in the eddying regime. The random phase of CIV "noise" can result in either high, small or even negative model-ARMOR3D correlations (from -0.45 to 0.8 for STMW temperature) depending on the ensemble member. Assessing a single eddying ocean simulation against ~~an observational reference~~ observational references should thus be done with care, all the more since ~~the latter reference~~ such references also contain random components, with an amplitude that ~~will be~~ is specific to the object of study.

The quantitative results of the present study may somewhat depend on certain model parameters and on our analysis technique. In particular, it is difficult to predict whether a finer model resolution may enhance STMW's intrinsic fractions R_σ (as found for sea level, see Sérazin et al., 2015) or barely impact them (as shown for AMOC, see Grégorio et al., 2015). We also made the classical assumption that the forced and intrinsic variabilities of STMW properties may be separated and quantified using ensemble means and ensemble anomalies; other approaches have been recently proposed to avoid this separation (see e.g. Fedele et al., 2021). More generally, alternative ensemble simulations and diagnostics could help refine the present results.

The impacts of CIV on STMW properties at eddy-permitting resolution are likely to exist as well in coupled ocean-atmosphere simulations, although experimental strategies allowing to quantify CIV impacts in a coupled context are not clear yet. In the meantime, prescribing the atmospheric forcing of an eddying ocean ensemble simulation as done here provides a natural and efficient means to study forced and intrinsic variabilities. In this forced ocean modelling context, the ensemble-mean forcing technique that we propose is designed to let CIV behave as freely as it may in an eddying ocean model coupled to the atmosphere, by removing an excessive damping of upper-ocean thermal intrinsic variability up to long timescales.

Previous studies have shown that beyond STMW properties, the interannual-to-multidecadal variability of several other climate-relevant oceanic indices are influenced by oceanic CIV, which is strongly underestimated in coarse-resolution ocean models such as those used in most CMIP-class climate models. The physical consistency of climate models may thus be

15

improved by taking CIV into account, either explicitly by using higher resolution ocean components, or by parameterizing the impacts of CIV in coarse ocean components.

References

375   Balmaseda, M., Hernandez, F., Storto, A., Palmer, M., Alves, O., Shi, L., Smith, G., Toyoda, T., Valdivieso, M., Barnier, B., Behringer, D., Boyer, T., Chang, Y.-S., Chepurin, G., Ferry, N., Forget, G., Fujii, Y., Good, S., Guinehut, S., Haines, K., Ishikawa, Y., Keeley, S., Köhl, A., Lee, T., Martin, M., Masina, S., Masuda, S., Meyssignac, B., Mogensen, K., Parent, L., Peterson, K., Tang, Y., Yin, Y., Vernieres, G., Wang, X., Waters, J., Wedd, R., Wang, O., Xue, Y., Chevallier, M., Lemieux, J.-F., Dupont, F., Kuragano, T., Kamachi, M., Awaji, T., Caltabiano, A., Wilmer-Becker, K., and Gaillard, F.: The Ocean Reanalyses Intercomparison Project (ORA-IP), Journal of Operational
380   Oceanography, 8, s80–s97, https://doi.org/10.1080/1755876X.2015.1022329, 2015.

Barnier, B., Siefridt, L., and Marchesiello, P.: Thermal forcing for a global ocean circulation model using a three-year climatology of ECMWF analyses, Journal of Marine Systems, 6, 363–380, https://doi.org/https://doi.org/10.1016/0924-7963(94)00034-9, 1995.

Bates, N. R.: Interannual variability of the oceanic CO2 sink in the subtropical gyre of the North Atlantic Ocean over the last 2 decades, Journal of Geophysical Research: Oceans, 112, https://doi.org/https://doi.org/10.1029/2006JC003759, 2007.

385   Bates, N. R., Pequignet, A. C., Johnson, R. J., and Gruber, N.: A short-term sink for atmospheric CO2 in subtropical mode water of the North Atlantic Ocean, Nature, 420, 489 – 493, https://doi.org/10.1029/2006JC003759, 2002.

Bessières, L., Leroux, S., Brankart, J.-M., Molines, J.-M., Moine, M.-P., Bouttier, P.-A., Penduff, T., Terray, L., Barnier, B., and Sérazin, G.: Development of a probabilistic ocean modelling system based on NEMO 3.5: application at eddying resolution, Geoscientific Model Development, 10, 1091–1106, https://doi.org/10.5194/gmd-10-1091-2017, 2017.

390   Billheimer, S. and Talley, L. D.: Near cessation of Eighteen Degree Water renewal in the western North Atlantic in the warm winter of 2011–2012, Journal of Geophysical Research: Oceans, 118, 6838–6853, https://doi.org/https://doi.org/10.1002/2013JC009024, 2013.

Billheimer, S. and Talley, L. D.: Annual cycle and destruction of Eighteen Degree Water, Journal of Geophysical Research: Oceans, 121, 6604–6617, https://doi.org/https://doi.org/10.1002/2016JC011799, 2016.

Brankart, J.-M.: Impact of uncertainties in the horizontal density gradient upon low resolution global ocean modelling, Ocean Modelling, 66,
395   64–76, https://doi.org/https://doi.org/10.1016/j.ocemod.2013.02.004, 2013.

Christiansen, B.: Analysis of Ensemble Mean Forecasts: The Blessings of High Dimensionality, Monthly Weather Review, 147, 1699 – 1712, https://doi.org/10.1175/MWR-D-18-0211.1, 2019.

Cleveland, W. S.: Robust Locally Weighted Regression and Smoothing Scatterplots, Journal of the American Statistical Association, 74, 829–836, http://www.jstor.org/stable/2286407, 1979.

400   Dewar, W. K.: Nonlinear Midlatitude Ocean Adjustment, Journal of Physical Oceanography, 33, 1057 – 1082, https://doi.org/10.1175/1520-0485(2003)033<1057:NMOA>2.0.CO;2, 2003.

Dong, S. and Kelly, K. A.: Heat Budget in the Gulf Stream Region: The Importance of Heat Storage and Advection, Journal of Physical Oceanography, 34, 1214 – 1231, https://doi.org/10.1175/1520-0485(2004)034<1214:HBITGS>2.0.CO;2, 2004.

Dong, S. and Kelly, K. A.: How Well Do Climate Models Reproduce North Atlantic Subtropical Mode Water?, Journal of Physical Oceanog-
405   raphy, 43, 2230–2244, https://doi.org/10.1175/JPO-D-12-0215.1, 2013.

Douglass, E. M., Jayne, S. R., Peacock, S., Bryan, F. O., and Maltrud, M. E.: Subtropical Mode Water Variability in a Climatologically Forced Model in the Northwestern Pacific Ocean, Journal of Physical Oceanography, 42, https://doi.org/10.1175/2011jpo4513.1, 2012.

Dussin, R., Barnier, B., Brodeau, L., , and Molines, J. M.: The Making Of the DRAKKAR FORCING SET DFS5, DRAKKAR/MyOcean Report 01-04-16, 2016.

410 Eade, R., Smith, D., Scaife, A., Wallace, E., Dunstone, N., Hermanson, L., and Robinson, N.: Do seasonal-to-decadal climate predictions underestimate the predictability of the real world?, Geophysical Research Letters, 41, 5620–5628, https://doi.org/https://doi.org/10.1002/2014GL061146, 2014.

Ertel, H.: On hydrodynamic eddy theorems, Physikalische Zeitschrift, 43, 526 – 529, 1942.

Evans, D. G., Toole, J., Forget, G., Zika, J. D., Naveira Garabato, A. C., Nurser, A. J. G., and Yu, L.: Recent Wind-Driven Variabil-
415 ity in Atlantic Water Mass Distribution and Meridional Overturning Circulation, Journal of Physical Oceanography, 47, 633–647, https://doi.org/10.1175/JPO-D-16-0089.1, 2017.

Fedele, G., Penduff, T., Pierini, S., Alvarez-Castro, M. C., Bellucci, A., and Masina, S.: Interannual to decadal variability of the Kuroshio extension: analyzing an ensemble of global hindcasts from a dynamical system viewpoint, Climate Dynamics, 57, 975–992, https://doi.org/10.1007/s00382-021-05751-7, 2021.

420 Feucher, C., Maze, G., and Mercier, H.: Mean Structure of the North Atlantic Subtropical Permanent Pycnocline from In Situ Observations, Journal of Atmospheric and Oceanic Technology, 33, 1285 – 1308, https://doi.org/https://doi.org/10.1175/JTECH-D-15-0192.1, 2016.

Feucher, C., Maze, G., and Mercier, H.: Subtropical Mode Water and Permanent Pycnocline Properties in the World Ocean, Journal of Geophysical Research: Oceans, 124, 1139–1154, https://doi.org/https://doi.org/10.1029/2018JC014526, 2019.

Forget, G., Maze, G., Buckley, M., and Marshall, J.: Estimated Seasonal Cycle of North Atlantic Eighteen Degree Water Volume, Journal of
425 Physical Oceanography, 41, 269 – 286, https://doi.org/10.1175/2010JPO4257.1, 2011.

Grégorio, S., Penduff, T., Sérazin, G., Molines, J.-M., Barnier, B., and Hirschi, J.: Intrinsic Variability of the Atlantic Merid-
ional Overturning Circulation at Interannual-to-Multidecadal Time Scales, Journal of Physical Oceanography, 45, 1929 – 1946, https://doi.org/https://doi.org/10.1175/JPO-D-14-0163.1, 2015.

Guinehut, S., Dhomps, A.-L., Larnicol, G., and Le Traon, P.-Y.: High resolution 3-D temperature and salinity fields derived from in situ and
430 satellite observations, Ocean Science, 8, 845–857, https://doi.org/10.5194/os-8-845-2012, 2012.

Haynes, P. H. and McIntyre, M. E.: On the Conservation and Impermeability Theorems for Potential Vorticity, Journal of Atmospheric Sciences, 47, 2021 – 2031, https://doi.org/10.1175/1520-0469(1990)047<2021:OTCAIT>2.0.CO;2, 1990.

Hazeleger, W. and Drijfhout, S. S.: A model study on internally generated variability in subtropical mode water formation, Journal of Geo-
physical Research, 105, 13,965–13,979, https://doi.org/10.1029/2000JC900041, provided by the SAO/NASA Astrophysics Data System,
435 2000.

Hochet, A., Huck, T., Arzel, O., Sévellec, F., de Verdière, A. C., Mazloff, M., and Cornuelle, B.: Direct Temporal Cascade of Temperature Variance in Eddy-Permitting Simulations of Multidecadal Variability, Journal of Climate, 33, 9409 – 9425, https://doi.org/10.1175/JCLI-D-19-0921.1, 2020.

Hogg, A. M., Penduff, T., Close, S. E., Dewar, W. K., Constantinou, N. C., and Martínez-Moreno, J.: Circumpolar Variations
440 in the Chaotic Nature of Southern Ocean Eddy Dynamics, Journal of Geophysical Research: Oceans, 127, e2022JC018 440, https://doi.org/https://doi.org/10.1029/2022JC018440, e2022JC018440 2022JC018440, 2022.

Jenkins, W. J. and Doney, S. C.: The subtropical nutrient spiral, Global Biogeochemical Cycles, 17, https://doi.org/https://doi.org/10.1029/2003GB002085, 2003.

Joyce, T. M.: New perspectives on eighteen-degree water formation in the North Atlantic, pp. 41–48, Springer Japan, Tokyo, ISBN 978-4-
445 431-54162-2, https://doi.org/10.1007/978-4-431-54162-2_3, 2013.

Joyce, T. M., Thomas, L. N., Dewar, W. K., and Girton, J. B.: Eighteen Degree Water formation within the Gulf Stream during CLIMODE, Deep Sea Research Part II: Topical Studies in Oceanography, 91, 1–10, https://doi.org/https://doi.org/10.1016/j.dsr2.2013.02.019, subtropical Mode Water in the North Atlantic Ocean, 2013.

Kelly, K. A. and Dong, S.: The contributions of atmosphere and ocean to North Atlantic Subtropical Mode Water volume anomalies, Deep Sea Research Part II: Topical Studies in Oceanography, 91, 111–127, https://doi.org/https://doi.org/10.1016/j.dsr2.2013.02.020, subtropical Mode Water in the North Atlantic Ocean, 2013.

Kelly, K. A., Small, R. J., Samelson, R. M., Qiu, B., Joyce, T. M., Kwon, Y.-O., and Cronin, M. F.: Western Boundary Currents and Frontal Air–Sea Interaction: Gulf Stream and Kuroshio Extension, Journal of Climate, 23, 5644 – 5667, https://doi.org/10.1175/2010JCLI3346.1, 2010.

Kwon, Y.-O. and Riser, S. C.: North Atlantic Subtropical Mode Water: A history of ocean-atmosphere interaction 1961–2000, Geophysical Research Letters, 31, https://doi.org/https://doi.org/10.1029/2004GL021116, 2004.

Leroux, S., Penduff, T., Bessières, L., Molines, J.-M., Brankart, J.-M., Sérazin, G., Barnier, B., and Terray, L.: Intrinsic and Atmospherically Forced Variability of the AMOC: Insights from a Large-Ensemble Ocean Hindcast, Journal of Climate, 31, 1183 – 1203, https://doi.org/10.1175/JCLI-D-17-0168.1, 2018.

Levitus, S., Boyer, T. P., Conkright, M. E., O'Brien, T., Antonov, J., Stephens, C., Stathoplos, L., Johnson, D., and Gelfeld, R.: World ocean database 1998. Volume 1, Introduction, NOAA Atlas NESDIS, 18, 346 pp, https://repository.library.noaa.gov/view/noaa/49345, 1998.

Li, K., Maze, G., and Mercier, H.: Ekman Transport as the Driver of Extreme Interannual Formation Rates of Eighteen Degree Water, Journal of Geophysical Research: Oceans, 127, e2021JC017 696, https://doi.org/10.1029/2021JC017696, e2021JC017696 2021JC017696, 2022.

Llovel, W., Kolodziejczyk, N., Close, S., Penduff, T., Molines, J.-M., and Terray, L.: Imprint of intrinsic ocean variability on decadal trends of regional sea level and ocean heat content using synthetic profiles, Environmental Research Letters, 17, 044 063, https://doi.org/10.1088/1748-9326/ac5f93, 2022.

Marshall, J., Jamous, D., and Nilsson, J.: Entry, Flux, and Exit of Potential Vorticity in Ocean Circulation, Journal of Physical Oceanography, 31, 777 – 789, https://doi.org/https://doi.org/10.1175/1520-0485(2001)031<0777:EFAEOP>2.0.CO;2, 2001.

Maze, G. and Marshall, J.: Diagnosing the Observed Seasonal Cycle of Atlantic Subtropical Mode Water Using Potential Vorticity and Its Attendant Theorems, Journal of Physical Oceanography, 41, 1986 – 1999, https://doi.org/10.1175/2011JPO4576.1, 2011.

Maze, G., Forget, G., Buckley, M., Marshall, J., and Cerovecki, I.: Using Transformation and Formation Maps to Study the Role of Air–Sea Heat Fluxes in North Atlantic Eighteen Degree Water Formation, Journal of Physical Oceanography, 39, 1818 – 1835, https://doi.org/10.1175/2009JPO3985.1, 2009.

Mulet, S., Rio, M.-H., Mignot, A., Guinehut, S., and Morrow, R.: A new estimate of the global 3D geostrophic ocean circulation based on satellite data and in-situ measurements, Deep Sea Research Part II: Topical Studies in Oceanography, 77-80, 70–81, https://doi.org/https://doi.org/10.1016/j.dsr2.2012.04.012, satellite Oceanography and Climate Change, 2012.

Palter, J. B., Lozier, M. S., and Barber, R. T.: The effect of advection on the nutrient reservoir in the North Atlantic subtropical gyre, Nature, 437, 687 – 692, https://doi.org/10.1038/nature03969, 2005.

Penduff, T., Juza, M., Brodeau, L., Smith, G. C., Barnier, B., Molines, J.-M., Treguier, A.-M., and Madec, G.: Impact of global ocean model resolution on sea-level variability with emphasis on interannual time scales, Ocean Science, 6, 269–284, https://doi.org/10.5194/os-6-269-2010, 2010.

Penduff, T., Juza, M., Barnier, B., Zika, J., Dewar, W. K., Treguier, A.-M., Molines, J.-M., and Audiffren, N.: Sea Level Expression of Intrinsic and Forced Ocean Variabilities at Interannual Time Scales, Journal of Climate, 24, 5652 – 5670, https://doi.org/10.1175/JCLI-D-11-00077.1, 2011.

485 Penduff, T., Terray, B. B. L., Bessières, L., Brankart, G. S. J.-M., Moine, M.-P., Molines, J.-M., and Brasseur, P.: Ensembles of eddying ocean simulations for climate, CLIVAR Exchanges No. 65, Vol. 19, No. 2., 2014.

Pérez, F. F., Mercier, H., Vázquez-Rodríguez, M., Lherminier, P., Velo, A., Pardo, P. C., Rosón, G., and Ríos, A. F.: Atlantic Ocean CO2 uptake reduced by weakening of the meridional overturning circulation, Nature Geoscience, 6, 146 – 152, https://doi.org/10.1038/ngeo1680, 2013.

490 Scaife, A. A. and Smith, D.: A signal-to-noise paradox in climate science, npj Climate and Atmospheric Science, 1, 28, https://doi.org/10.1038/s41612-018-0038-4, 2018.

Sinha, A., Callies, J., and Menemenlis, D.: Do Submesoscales Affect the Large-Scale Structure of the Upper Ocean?, Journal of Physical Oceanography, 53, 1025–1040, https://doi.org/https://doi.org/10.1175/JPO-D-22-0129.1, 2023.

Speer, K. and Tziperman, E.: Rates of Water Mass Formation in the North Atlantic Ocean, Journal of Physical Oceanography, 22, 93 – 104,
495 https://doi.org/10.1175/1520-0485(1992)022<0093:ROWMFI>2.0.CO;2, 1992.

Stevens, S. W., Johnson, R. J., Maze, G., and Bates, N. R.: A recent decline in North Atlantic subtropical mode water formation, Nature Climate Change, 10, 335–341, https://doi.org/https://doi.org/10.1038/s41558-020-0722-3, 2020.

Sérazin, G., Penduff, T., Grégorio, S., Barnier, B., Molines, J.-M., and Terray, L.: Intrinsic Variability of Sea Level from Global 1/12° Simulations: Spatiotemporal Scales, Journal of Climate, 28, 4279–4292, http://www.jstor.org/stable/26195138, 2015.

500 Sérazin, G., Jaymond, A., Leroux, S., Penduff, T., Bessières, L., Llovel, W., Barnier, B., Molines, J.-M., and Terray, L.: A global probabilistic study of the ocean heat content low-frequency variability: Atmospheric forcing versus oceanic chaos, Geophysical Research Letters, 44, 5580–5589, https://doi.org/https://doi.org/10.1002/2017GL073026, 2017.

Sérazin, G., Penduff, T., Barnier, B., Molines, J.-M., Arbic, B. K., Müller, M., and Terray, L.: Inverse Cascades of Kinetic Energy as a Source of Intrinsic Variability: A Global OGCM Study, Journal of Physical Oceanography, 48, 1385 – 1408, https://doi.org/10.1175/JPO-D-17-505 0136.1, 2018.

Taylor, K. E.: Summarizing multiple aspects of model performance in a single diagram, Journal of Geophysical Research: Atmospheres, 106, 7183–7192, https://doi.org/https://doi.org/10.1029/2000JD900719, 2001.

Wenegrat, J. O., Thomas, L. N., Gula, J., and McWilliams, J. C.: Effects of the Submesoscale on the Potential Vorticity Budget of Ocean Mode Waters, Journal of Physical Oceanography, 48, 2141 – 2165, https://doi.org/10.1175/JPO-D-17-0219.1, 2018.

510 Worthington, L.: The 18° water in the Sargasso Sea, Deep Sea Research (1953), 5, 297–305, https://doi.org/https://doi.org/10.1016/0146-6313(58)90026-1, 1958.

Worthington, L.: On the North Atlantic Circulation, no. n° 6 in (Contrib. from Woods Hole Ocean. Inst), Johns Hopkins University Press, ISBN 9780801817427, https://books.google.fr/books?id=RVFVAAAAMAAJ, 1976.

Zanna, L., Brankart, J. M., Huber, M., Leroux, S., Penduff, T., and Williams, P. D.: Uncertainty and scale interactions in ocean ensem-515 bles: From seasonal forecasts to multidecadal climate predictions, Quarterly Journal of the Royal Meteorological Society, 145, 160–175, https://doi.org/https://doi.org/10.1002/qj.3397, 2019.
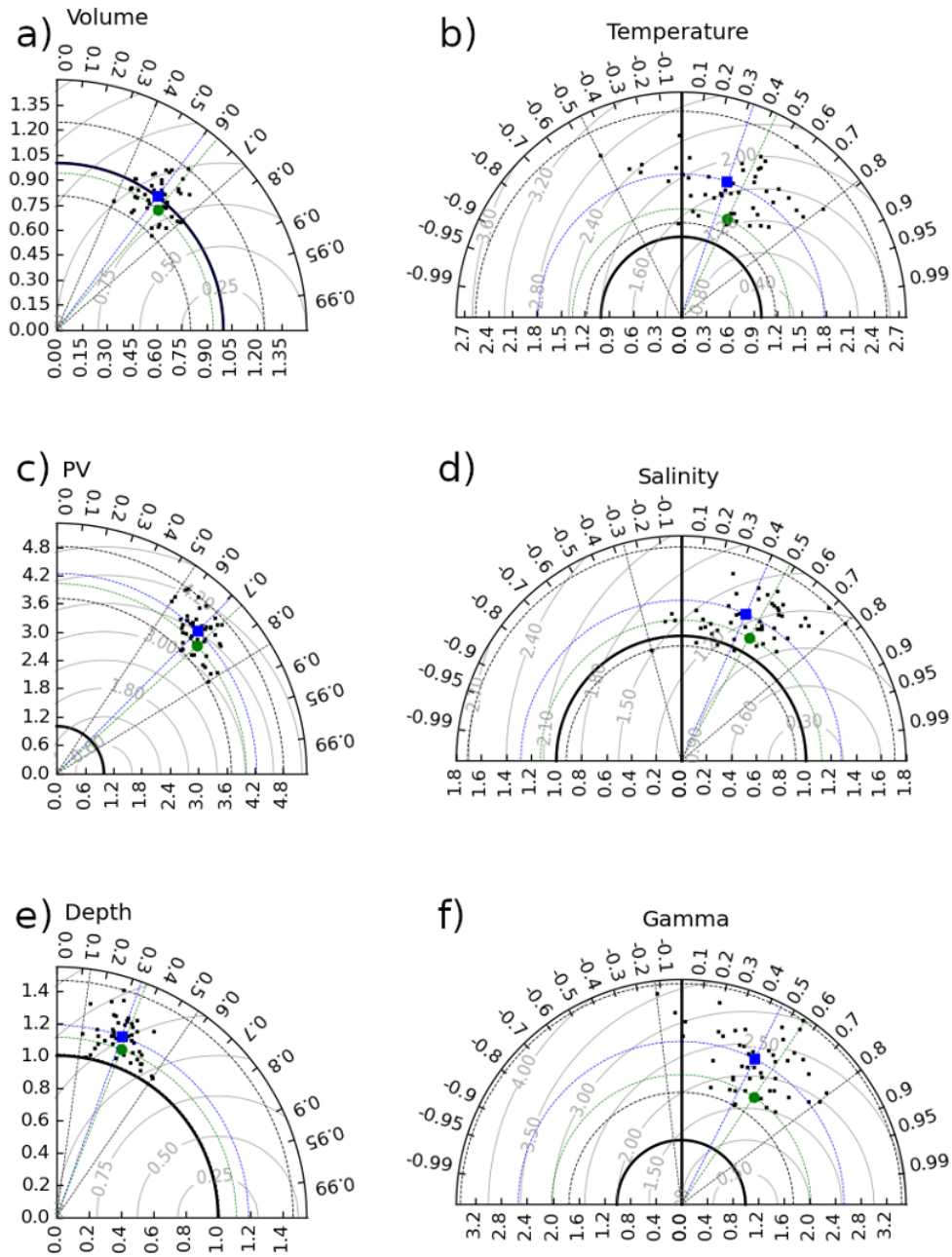
Figure 5. Taylor diagrams comparing the interannual fluctuations of STMW properties in the reference (ARMOR3D time series) and in each ensemble member (total variabilities, black dots), and in their ensemble mean (forced variabilities, green circles). Blue squares show the center of gravity of black dots. The distance between each dot and the origin gives the ratio of simulated and reference STDs; the angle between the latter line and the horizontal axis gives the temporal correlation between simulated and reference time series; the distance between dots and the (1,0) point gives the RMS difference between the latter time series. Thick black lines show unity STD ratios; grey dotted lines show the range of correlations and STD ratios for black dots; blue and green dotted lines show the coordinates of blue squares and green circles.
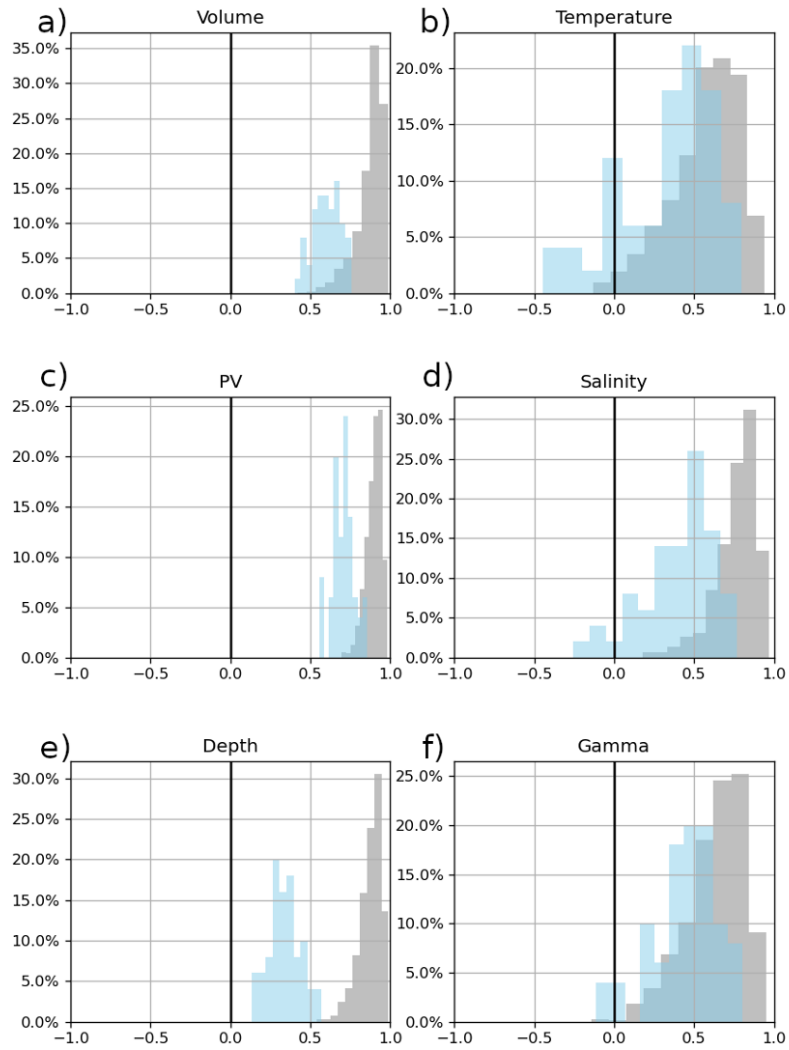
Figure 6. Distributions of various correlation coefficients using the interannual fluctuations of STMW properties in the 50 ensemble members as references. The distributions show their correlations with the corresponding time series in all other ensemble members (grey), and in ARMOR3D (blue).